Iranian Journal of Chemical Engineering

Journal Homepage: www.ijche.com

pISSN: 1735-5397
eISSN: 2008-2355

Green Synthesis of AuNPs using *Teucrium polium* Extract: A Dual-Action Platform for Antimicrobial Activity and Phytochemical Enhancement

Samer Asadi [1]*, ***Ehsan Dahaz***[2], ***Somayeh Lashgari***[3]

[1] *Department of Chemical Engineering, Petroleum University of Technology (PUT), Abadan, Iran*
[2] *Department of Chemical Engineering, Kherad Institute of Higher Education, Bushehr, Iran*
[3] *Iran Polymer and Petrochemical Institute, P.O.: 14965-115, Tehran, Iran*

ARTICLE INFO

Article type:
Research article

Article history:
Received: 2026-02-16
Revised: 2026-03-04
Accepted: 2026-03-20
Available online: 2026-03-29

Keywords:
AuNPs,
T. polium plant extract,
Antibacterial,
Antifungal,
Antioxidant activity,
Reducing power

ABSTRACT

In this research, gold nanoparticles (AuNPs) were synthesized for the first time utilizing the extract of Teucrium polium. The study evaluated the antimicrobial potential of both methanolic and aqueous extracts of T. polium, alongside the synthesized AuNPs. Furthermore, the impact of varying AuNP concentrations on the phytochemical characteristics of the plant extract was analyzed. The successful fabrication of AuNPs was verified through a comprehensive suite of characterization techniques, including UV-Vis spectroscopy, XRD, TEM, SEM, and FTIR. Morphological analysis via SEM and TEM revealed spherical nanoparticles with a mean diameter of 22.89 nm, while the UV-Vis spectrum exhibited a characteristic surface plasmon resonance (SPR) peak at 420 nm. The reaction reached its optimum efficiency at pH 5. Antimicrobial assays indicated that the methanolic extract possessed superior antibacterial and antifungal properties compared to the aqueous version, yielding maximum inhibition zones for Escherichia coli (14±1.4 mm) and Aspergillus niger (15±0.7 mm). Additionally, the AuNPs demonstrated notable efficacy against gram-negative bacteria, with the highest inhibition observed for E. coli (18±0.7 mm) and A. niger (20±0.9 mm). Regarding the antioxidant capacity and reducing power (phenolic flavonoid content), a concentration-dependent increase was observed up to 60 ppm (IC50=9.94 µg/mL; reducing power= 16.85 mMFe2+/mg sample), followed by a decline at concentrations exceeding this threshold.

DOI: 10.22034/ijche.2026.579473.1589 URL: https://www.ijche.com/article_245510.html

*Corresponding author: samer.asadi@put.ac.ir

1. Introduction

The global surge in antibiotic-resistant bacterial strains has evolved into a formidable public health crisis, undermining the effectiveness of traditional antimicrobial treatments and placing an immense burden on international healthcare infrastructures. Consequently, the urgent development of innovative therapeutic modalities characterized by superior stability and heightened efficacy is imperative to counteract the proliferation of antimicrobial resistance (AMR) [1-3]. In this context, medicinal plants offer a promising reservoir of bioactive compounds. Phytochemicals, particularly phenolic compounds, exhibit significant antimicrobial, antiviral, and anti-inflammatory properties, often presenting fewer side effects compared to synthetic drugs [4,5].

Integrating nanotechnology with phytochemistry has opened new avenues for combating resistant pathogens. Metal nanoparticles, specifically gold nanoparticles (AuNPs), have gained prominence due to their exceptional chemical stability, low toxicity, and unique optical properties [6,7]. The potent antimicrobial capacity of AuNPs against a broad spectrum of microorganisms, notably *Escherichia coli*, *Pseudomonas aeruginosa*, *Staphylococcus aureus*, and *Bacillus subtilis*, is primarily driven by their high surface-area-to-volume ratio, which promotes superior engagement with the membranes of these pathogens [8, 9].

Although conventional physical and chemical approaches are widely utilized, their reliance on hazardous chemicals and significant energy requirements is a major drawback. In response, the use of plant extracts for "green synthesis" has gained prominence as an eco-friendly and biologically compatible substitute. The dual functionality of plant-derived phytochemicals as reducing and stabilizing agents facilitates a greener synthesis route, effectively eliminating the requirement for hazardous reagents while curtailing overall expenses [10, 11]. Compared to microbial synthesis, plant-mediated synthesis is more efficient, time-saving, and scalable, as it bypasses the need for complex cell culture processes [12]. Significant antibacterial effects, particularly against Gram-positive bacteria, were observed in AuNPs synthesized via *Andrographis paniculata* and *Anemopsis californica*, as reported in recent literature [13,14].

Despite the known benefits of both medicinal plant extracts and AuNPs, the synergistic potential of combining them using *Teucrium polium (T. polium)* remains unexplored. *T. polium* (***Lamiaceae***) is widely distributed in southwest Asia, particularly in Iran, and is traditionally recognized for its diverse pharmacological properties, including gastrointestinal and anti-inflammatory effects [15]. To date, no research has examined how this plant functions as a reducing agent in the synthesis of AuNPs, nor has the influence of such nanoparticles on the plant's own phytochemical properties been evaluated.

Accordingly, the current work aims to synthesize AuNPs through a green route mediated by *T. polium* extract, addressing a gap in the current body of literature. In this study, the antibacterial and antifungal properties of the resulting AuNPs are compared against the activities of the original aqueous and methanolic extracts. Furthermore, this study employs a novel strategy by evaluating the impact of different biosynthesized AuNP concentrations on the antioxidant capacity and reducing ability of the plant extract. This investigation into the bidirectional effect reveals new ways to augment the bioactivity of plant-based

extracts using nanoparticles synthesized from the same source.

Figure 1. The *T. polium* plant.

2. Experimental

2.1. Chemicals

High-purity reagents were procured from Merck for all experimental procedures. These included 2,2-diphenyl-1-picrylhydrazyl (DPPH), ascorbic acid (ASA) (100%), butylated hydroxytoluene (BHT) (99.99%), and gallic acid (99%). Additionally, various salts and acids were utilized, such as sodium hydroxide (98%), hydrochloric acid (37%), acetic acid (99.9%), iron(III) chloride (99%), iron(II) chloride (99%), aluminum chloride (98%), sodium carbonate (98%), and sodium acetate (98%). Other essential chemicals employed were quercetin, Folin's reagent, iron sulfate (99.95%), 2,4,6-tri(2-pyridyl)-s-triazine (TPTZ) (99%), gold(III) chloride (HAuCl4), along with methanol (99.9%), ethanol, and distilled water.

2.2. Devices

Absorption spectra were recorded using a Unico 2100 UV-Vis spectrophotometer, while pH values were determined with a pH lab 827 meter. A Kern digital balance (precision: 0.0001 g) was employed for accurate weighing. For sample processing, a Sigma 2-7 centrifuge was used for separation, an SB-100D ultrasonic bath for dissolution, and a Clevenger-type apparatus for the extraction of essential oils. The latter were further analyzed via a GC-7890B gas chromatography system coupled with an MS5977A mass spectrometer. Structural and morphological characterizations were performed using a PHILIPS PW1730 X-ray diffractometer (XRD), a Thermo AVATAR Fourier Transform Infrared (FT-IR) spectrometer, a TESCAN VEGA3 scanning electron microscope (SEM), and a Philips Holland CM120 transmission electron microscope (TEM).

2.3. Water extract preparation

Aerial parts of *T. polium* were harvested from a 5 km^2 area within the mountainous terrains of Dashti County, Bushehr Province, Iran [15]. The collection process was conducted by Dr. Mozaffarian, and the resulting botanical identity was formally verified. To ensure authenticity, a voucher specimen was deposited in the herbarium of the Research Institute of Forests and Rangelands (TARI) under the registration number 87532, from which the aqueous extract was subsequently prepared.

To obtain a pure extract for the reduction of gold ions, 10 g of powdered plant material was weighed and dispersed in 100 mL of doubly distilled deionized water. The mixture was stirred using an electric mixer at 30–40 °C for 30 min. After cooling to room temperature, the solution was filtered through Whatman No. 42 filter paper. To eliminate any remaining particulate matter or impurities, the resulting filtrate was centrifuged at 10,000 rpm for 10 min.

To ensure reproducibility and account for plant-to-plant variability, three independent extractions were performed using separate batches of *T. polium* plant material, each collected from distinct plants in Dashti

County, Bushehr Province,. Each batch (10 g) was processed as described above, and the resulting extracts were used individually for nanoparticle synthesis.

AuNPs were prepared by adding 1 mL of the plant's aqueous extract to 8 mL of 1 mM HAuCl4 solution. After 30 min of stirring at 150 rpm and an hour of incubation at ambient temperature, the solution turned purple, indicating successful AuNP synthesis (Fig. 2). The aqueous extract functioned as a dual-purpose reducing and capping agent.

To confirm the reproducibility of the synthesis method, three independent syntheses were conducted, each using a distinct extract from a different *T. polium* plant batch. Each synthesis followed the optimized conditions (1 mL extract + 8 mL 1 mM $HAuCl_4$, pH 5, 150 rpm, 30 min). The nanoparticles were characterized by UV-Vis spectroscopy (SPR peak) and TEM (size and morphology), with results summarized in Table 4 (Section 3.9).

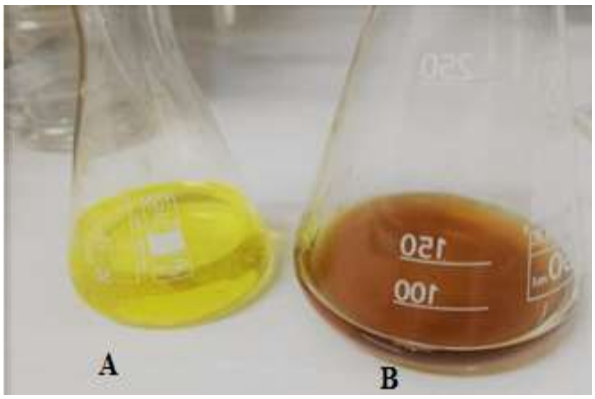

Figure 2. Visual appearance of the *T. polium* aqueous extract (A) prior to and (B) following the addition of 1 mM $HAuCl_4$ solution.

2.5. pH Optimization of the reaction medium

To determine the ideal acidity for AuNPs synthesis, a series of mixtures were prepared by combining 1 mL of *T. polium* extract with 8 mL of 1 mM gold salt solution, adjusting the pH levels to 2, 3, 4, 5, 6, and 8 (as detailed in Table 1). The pH values were precisely controlled using 0.1 M solutions of HCl and NaOH. Following the recording of absorption spectra via UV-Vis spectroscopy for each sample, the optimal pH was identified. As evidenced by the data in Table 1, the maximum absorption intensity was observed at pH 5, suggesting that this specific acidity promotes the formation of nanoparticles with superior quality and optimal concentration.

The pH affects nanoparticle size, shape, and stability. At pH=5, precursor protonation promotes controlled nucleation, yielding monodisperse nanoparticles with a strong surface plasmon resonance, as evident from the sharp UV-Vis peak. A pH lower than 5 leads to irregular particles due to altered kinetics. This aligns with prior studies [16]. Thus, pH 5 was chosen for optimal nanoparticle quality.

Table 1.
pH adjustment parameters employed for the optimized synthesis of AuNPs.

Soluble Series	Vol. of $HAuCl_4$ Solution (mL)	Extract Volume (mL)	pH	Total volume (mL)	Abs.
1	8	1	2	10	0.30
2	8	1	3	10	0.83
3	8	1	4	10	0.86
4	8	1	5	10	1.91
5	8	1	6	10	1.07
6	8	1	8	10	0.19

2.6. Evaluation of antimicrobial activity using aqueous and methanolic plant extracts

To evaluate the antimicrobial potential of *T. polium*, aqueous and methanolic extracts were synthesized. Briefly, 10 g of the powdered plant material was immersed in 100 mL of

either distilled water or methanol and subjected to continuous agitation on a shaker for 24 hours. The resulting mixtures were filtered using Whatman No. 42 filter paper. To ensure the removal of any remaining debris or impurities, the filtrates were centrifuged at 10,000 rpm for 15 minutes. Finally, the purified extracts were kept refrigerated at 4°C until further analysis.

2.7. Evaluation of antimicrobial activity

To investigate the antimicrobial properties of the synthesized AuNPs and the plant extracts (aqueous and methanolic), the disk diffusion method was employed following CLSI guidelines. A panel of microorganisms was used, comprising *Staphylococcus aureus*, *Bacillus cereus* (Gram-positive), *Escherichia coli*, *Salmonella typhimurium* (Gram-negative), and the fungi *Aspergillus niger* and *Candida albicans*. All strains were first cultivated in Nutrient Broth for 24 hours at 37°C with a shaking speed of 200 rpm. After incubation, the turbidity of the suspensions was adjusted to match the 0.5 McFarland standard (approximately 1.5×10^8 CFU/mL) via spectrophotometric analysis. Following this, the microorganisms were inoculated onto Mueller-Hinton Agar (MHA) plates. For the assay, 20 µL of AuNPs (100 µg/mL), aqueous extract, and methanolic extract were applied to sterile 6 mm paper discs. Negative controls consisted of methanol and distilled water for the corresponding extracts. For positive control, commercial antibiotic discs containing ampicillin, gentamicin, and clotrimazole were employed. Incubation of the plates was carried out at 37°C for a period of 24–48 h. A digital caliper was employed to determine the inhibition zone diameters (mm). To guarantee both technical and biological reproducibility, each assay was conducted in triplicate (n=3). Statistical analysis was performed via one-way analysis of variance (ANOVA) using SPSS software (v26), where a p-value below 0.05 was defined as the threshold for statistical significance.

2.8. Effect of AuNPs on phytochemical properties of *T. polium* plant

To evaluate the potential of AuNPs as biological elicitors for enhancing the production of secondary metabolites, a foliar spray treatment was applied to the aerial organs of *T. polium* prior to the flowering stage. To synthesize AuNPs, 1 mL of the aqueous extract was introduced into 8 mL of a 1 mM $HAuCl_4$ solution, maintaining the pH at 5.0 to ensure optimal conditions. The concentration (C) of the resulting nanoparticles was subsequently calculated utilizing Equation (1). Furthermore, the mean number of gold atoms constituting each nanoparticle (N) was estimated based on the average particle diameter obtained from TEM analysis. Consequently, the concentration of the AuNPs was determined to be approximately 315 ppm, which served as the stock solution. From this stock, a series of dilutions (0, 20, 40, 60, and 80 ppm) were prepared and applied as a foliar spray to the aerial parts of the plants over a three-week period.

It should be noted that, as part of a preliminary screening approach to assess the efficacy of these elicitors, the antimicrobial and phytochemical assays were performed as single measurements for each treatment.

$$C = N_{total} / N * V \quad (1)$$

N_{total}: The sum of gold atoms

N: The average number of gold atoms per nanoparticle

V: The final volume

The equation (2) is used to obtain the average number of gold atoms in each nanoparticle (N).

$$N = (N_A * \pi * D^3 * \rho / 6M) \quad (2)$$

N_A: Avogadro number

π: The number pi

D: Medium Diameter of Nanoparticles

ρ: : Density of gold atom (g/cm^3) (19.3 g/cm^3)

M: Atomic weight (196.96 g/gmole)

3. Results and discussion

3.1. UV-Vis analysis results

The synthesis was driven by the interaction between Au^+ ions and the reducing agents present within the plant aqueous extract, which triggered the reduction of gold nitrate salts. The successful conversion of Au^+ ions into AuNPs was visually confirmed by a distinct color shift in the reaction mixture. This phenomenon took place roughly five minutes following the initiation of the reaction. The UV-Vis spectra for the aqueous extract of *T. polium* and the mixture of the extract with $HAuCl_4$ are illustrated in Fig. 3(a) and (b), respectively. A characteristic absorption maximum was detected at approximately 420 nm, providing evidence for the successful formation of AuNPs [17]. Considering that the UV-Vis peak for synthesized AuNPs typically appears in the range of 520-560 nm, the observed difference could be attributed to the distinct environment provided by the *T. polium aqueous* extract surrounding the synthesized nanoparticles. As shown in Fig. 3a, the UV-Vis absorption peak of the plant *aqueous* extract was observed in the wavelength range of 270 to 450 nm. Upon addition of the $HAuCl_4$ solution (Fig. 3b), the absorption rate decreased, and a peak emerged at a wavelength of 420 nm. This shift could be due to the separation of various functional groups (stabilizers and reducing agents) from the extract and their subsequent deposition on the surface of the nanoparticles, imparting a plant-like nature to the nanoparticles. Consequently, the peak position shifted from 520 to 420 nm [18, 19]. Furthermore, the peaks observed at frequencies of 295 and 355 nm may be related to the phytochemical compounds present in the plant extract surrounding the synthesized AuNPs.

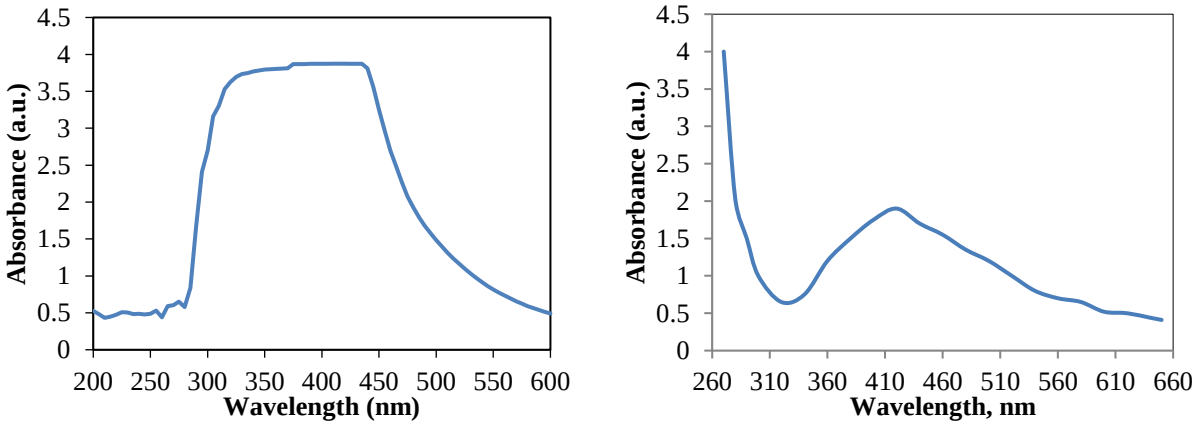

(a) **(b)**

Figure 3. UV-Vis spectroscopic analysis plot of (a) *T. polium* plant extract and (b) Synthesized AuNPs using *T. polium* aqueous extract.

3.2. XRD analysis results

The crystallinity of the AuNPs, produced via a green synthesis route, is confirmed by the XRD diffraction pattern displayed in Fig. 4.The crystalline nature of the synthesized AuNPs was validated through XRD analysis, where the emergence of diffraction peaks at 2θ values of 38.04°, 44.5°, 64°, and 77.7° corresponds to the (111), (200), (220), and (311) planes, respectively. These results are in full agreement with the standard FCC lattice of elemental gold (JCPDS card no. 04-0784), confirming a highly ordered crystalline phase [20]. Notably, the XRD pattern is devoid of any extraneous peaks, demonstrating that the *T. polium* extract effectively reduces gold ions without introducing crystalline impurities or secondary phases. Based on the Debye-Scherrer formula, the mean crystallite size was determined to be 22.8 nm [21], a dimension that typically enhances surface reactivity and suitability for biomedical or electronic integration. Furthermore, the interplanar spacing (d-spacing) for the (111) reflection was calculated as ≈0.25 nm, further reinforcing the authenticity of the FCC structure. These findings collectively underscore the efficacy of the green synthesis route in producing high-purity, structurally sound gold nanoparticles.

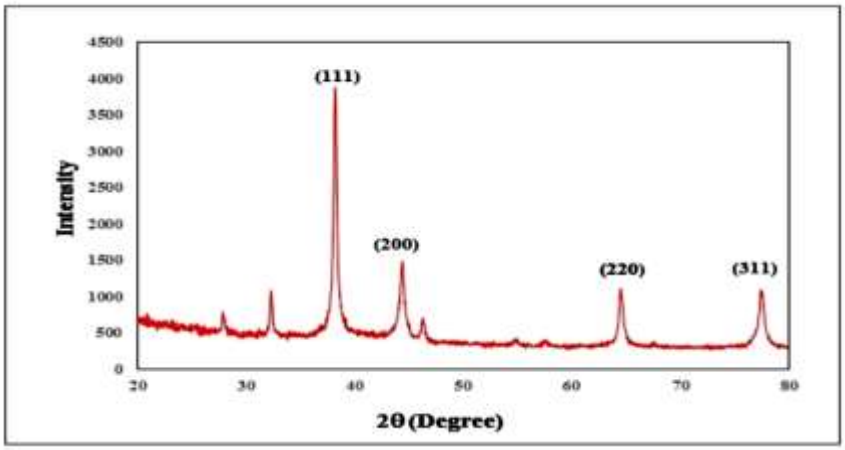

Figure 4. XRD analysis of synthesized AuNPs.

3.3. FTIR analysis results

The molecular coordination between the synthesized AuNPs and the biological capping agents was analyzed via FTIR spectroscopy (Fig. 5) [22-24]. Specifically, the transition of the O-H absorption band from 3438 to 3428 cm^{-1} serves as evidence for the strong interaction of *T. polium* phenolic compounds with the gold nanoparticle surface [25]. The stabilization of the nanoparticles is attributed to the emergence of a distinct chemical environment or the establishment of new bonds, as evidenced by this shift.

Comparison between the spectra of the plant extract and the synthesized AuNPs revealed overlapping absorption peaks at 2929, 1624, 1389, and 1278 cm^{-1}, signifying that functional moieties such as C-H, C=O, C-N, and type I amide remained intact post-synthesis [26, 27]. Such groups are hypothesized to facilitate the capping and stabilization of the AuNPs, thereby hindering aggregation and promoting a homogeneous size distribution.

The biocompatibility and potential for biomedical applications are enhanced by the attachment of plant-derived organic moieties to the AuNP surface, which is evidenced by

the characteristic C-O-C (ether) absorption bands observed at 1042 and 1058 cm^{-1} [27]. The synthesis of AuNPs via the aqueous extract of T. polium was validated by FTIR analysis, which underscored how plant-derived constituents are essential for ensuring the stability and functional properties of the resulting nanoparticles.

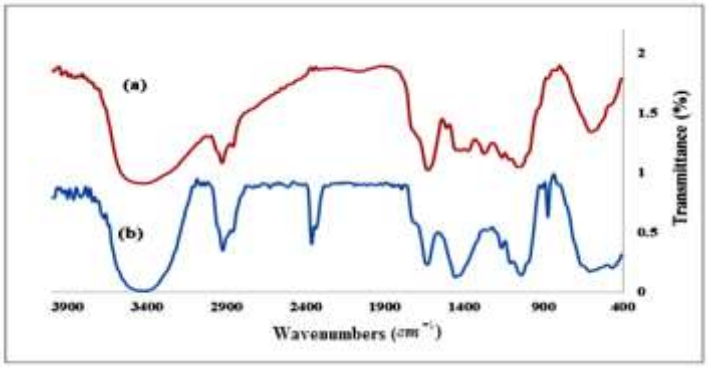

Figure 5. Comparison of FTIR spectra for (a) the aqueous extract of *T. polium* and (b) the resulting AuNPs.

3.4. SEM analysis results

The three-dimensional architecture of the synthesized AuNPs is illustrated in the SEM images (Fig. 6). The nanoparticles exhibit a distinct spherical morphology, a characteristic highly valued in nanotechnology for providing an optimized surface-to-volume ratio. Such a geometry is particularly beneficial for drug delivery systems, as consistent size and shape allow for more precise regulation of the release kinetics of therapeutic agents. While some agglomerations are evident a frequent occurrence in nanoparticle fabrication—these can be readily mitigated through sonication. Furthermore, the SEM data reflects the efficiency of the synthesis approach; the observed uniformity in particle dimensions suggests a well-controlled process, which is fundamental for achieving reproducibility and reliability in future applications.

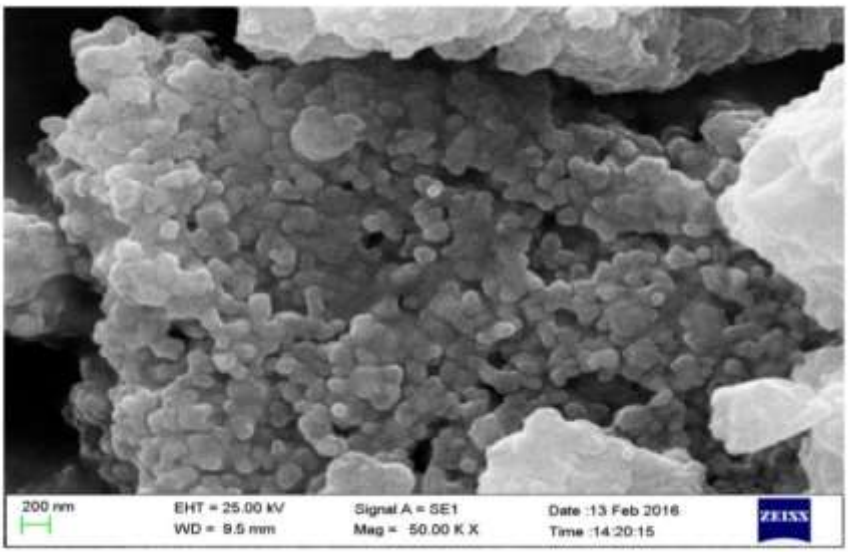

Figure 6. SEM micrograph of synthesized AuNPs.

3.5. TEM analysis results

The TEM micrographs of the AuNPs, synthesized via *T. polium* extract, are displayed in Fig. 7, confirming their spherical geometry and a diameter remaining below 50 nm. To further evaluate the size uniformity, a distribution histogram was generated for a random selection of 582 nanoparticles (Fig. 8). The analysis reveals a mean particle diameter of 22.89 nm, with a narrow size distribution indicated by a standard deviation of 0.3 nm.

The morphology and uniformity of the synthesized nanoparticles were effectively evaluated through TEM imaging. The observed spherical shape is particularly beneficial for various applications, as it ensures symmetrical properties and a balanced distribution of the surface area. Furthermore, the size distribution histogram demonstrates a high degree of consistency, which is a prerequisite for ensuring reproducibility in both academic research and industrial scales. Given that the nanoparticles are smaller than 50 nm, they are ideally suited for high-precision operations, such as sensing and targeted drug delivery, where a high surface-to-volume ratio is essential. It should be noted that the observed variations in particle size between TEM and SEM measurements can be attributed to differences in imaging methodologies and sample preparation protocols [26].

The difference between the average particle size from TEM (22.89 nm) and crystallite size from XRD (2.5 nm) arises because TEM measures overall nanoparticle size, while XRD estimates individual crystalline domain size within particles. This indicates each nanoparticle consists of multiple smaller crystallites. Additionally, particle aggregation and surface layers cause the larger TEM-observed size compared to XRD.

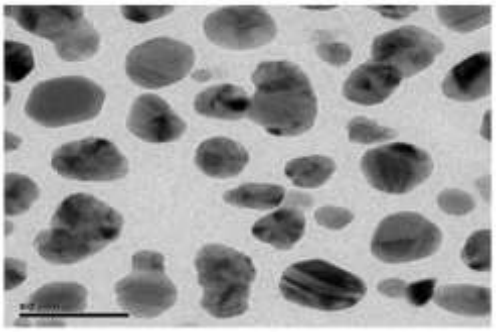

Figure 7. TEM Image of Synthesized AuNPs.

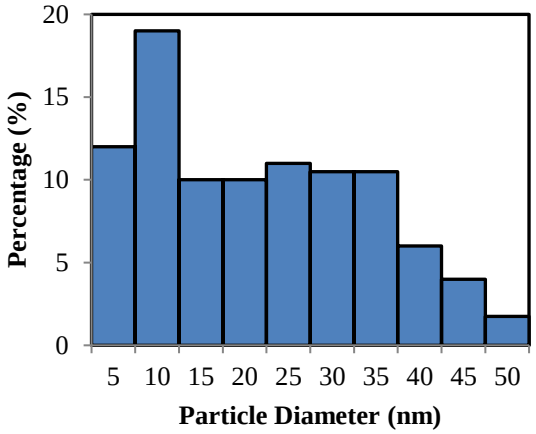

Figure 8. Particle size distribution of AuNPs fabricated via *T. polium* plant extract, represented as a histogram.

3.6. Evaluation of the antimicrobial potential of *T. polium* aqueous and methanolic extracts alongside synthesized AuNPs

This study investigated the antibacterial and antifungal properties of both the plant extracts and the synthesized gold nanoparticles, utilizing ampicillin, gentamicin, and clotrimazole as standard reference controls. The findings reveal that both the extracts and the nanoparticles exhibit significant inhibitory effects against the evaluated pathogens, highlighting their promising potential as viable alternative antimicrobial agents.

As illustrated in Fig. 9 and Table 2, the synthesized AuNPs outperformed the aqueous and methanolic extracts in terms of their antimicrobial and antifungal potency.The antimicrobial activity of synthesized AuNPs

aligns with previous reports on plant-based AuNPs. Franzolin et al. (2022) demonstrated AuNPs prepared using plant extracts exhibited inhibition zones up to 18±0.7 mm against *Escherichia coli* and notable antifungal effects, comparable to our findings of 18±0.7 mm and 20±0.9 mm inhibition zones against *E. coli* and *Aspergillus niger*, respectively [27]. This similarity supports combining medicinal plant extracts, such as *Teucrium polium*, with AuNPs to enhance antimicrobial potency. Furthermore as illustrated in Table 2, a progressive increase in antibacterial activity was observed from the aqueous extract to the methanolic extract, with the synthesized nanoparticles exhibiting the highest inhibitory effect.

The superior antimicrobial performance of the AuNPs likely stems from the synergistic interaction between the AuNPs and the *T. polium* extract. Such findings highlight the potential of merging conventional herbal medicine with nanotechnology to develop highly effective antimicrobial agents.

As seen in Table 2, synthesized AuNPs exhibit superior antibacterial performance to aqueous and methanolic extracts (larger growth inhibition zone diameter) against all microorganisms. Furthermore, results indicate antibiotics have limited effectiveness against certain microorganisms, whereas synthesized AuNPs are effective against almost all tested microorganisms. This may be due to nanoparticles' small size, high specific surface area, and gold type. Among antibiotics, Gentamicin (inhibition zone: 26-29 mm) shows optimal performance, making it a good option for combining with synthesized AuNPs to enhance antimicrobial efficacy. This highlights nanoparticles' potential as effective antimicrobial agents, overcoming traditional antibiotics' limitations. Moreover, the methanolic extract demonstrated superior antibacterial potency over the aqueous one. This disparity is probably attributable to the enhanced capacity of methanol to isolate bioactive constituents from the plant material.

However, the synthesized nanoparticles demonstrated a significantly more potent antibacterial effect than both extracts, including the methanolic one. This suggests that the enhanced antimicrobial activity is not merely a result of the solvent or the plant extract, but is primarily attributed to the formation of nanoparticles and the potential synergistic effect between the nanoparticles and the bioactive molecules.

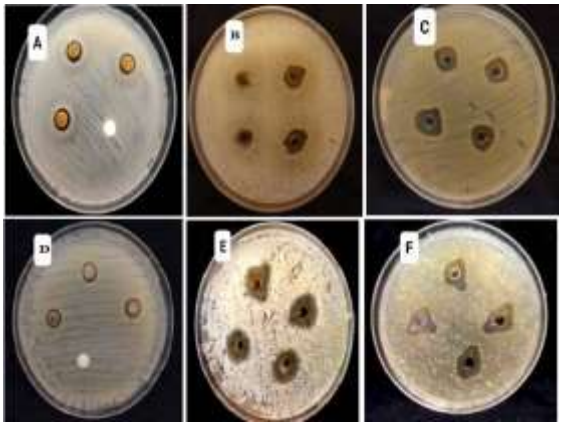

Figure 9. Antimicrobial activity of the synthesized AuNPs against various pathogens: (A) *Escherichia coli*, (B) *Salmonella Typhimurium*, (C) *Staphylococcus aureus*, (D) *Bacillus cereus*, (E) *Aspergillus niger*, and (F) *Candida albicans*.

Table 2.
Comparative analysis of antimicrobial efficacy: Synthesized AuNPs, aqueous and methanolic *T. polium* extracts, and standard antibiotics.*Data are presented as mean ± SD (n=3). Statistical significance was determined by one-way ANOVA ($p < 0.05$).

Microorganism	The diameter of the growth inhibition zone (mm)					
	Biosynthesized Au NPs	Aqueous Extract	Methanolic Extract	Gentamicin	Ampicillin	Clotrimazole
Escherichia coli	18±0.7	6±0.2	14±1.4	28	26	-
Salmonella Typhimurium	16±1.4	6±0.7	11±0.5	29	27	-
Staphylococcus aureus	14±0.6	8±0.5	13±0.2	26	25	-
Bacillus cereus	15±0.2	7±0.4	12±0.9	27	27	-
Aspergillus niger	20±0.9	10±1.3	15±0.7	-	-	30
Candida albicans	19±1.2	9±0.6	13±0.8	-	-	28

3.7. Impact of AuNPs on the phytochemical profile of T. polium extracts

To determine the chemical constituents of the *T. polium* essential oil, GC-MS analysis was performed following extraction with a Clevenger-type apparatus; these findings are detailed in Table 3. It was observed that the integration of AuNPs at different concentrations (ranging from 0 to 80 ppm) notably altered not only the total oil yield but also the distribution of its specific chemical components. The oil yield for the respective concentrations was recorded as 1.10, 0.118, 0.125, 0.133, 0.151, and 0.113%.

Figure 10 illustrates the comparative percentage of major constituents in the essential oil under the influence of different AuNP concentrations. A notable increase in the content of geranyl acetate was observed, peaking at 12.418% in the 60-ppm treatment, compared to 8.131% in the control (0 ppm). Similarly, Citral (E) showed a significant upward trend, reaching its maximum concentration (33.075%) at 60 ppm. For Citral (Z), the highest percentage was also recorded at 60 ppm (23.281%), although this increase was not statistically significant compared to the control. In contrast, Piperitone reached its peak at a lower concentration of 20 ppm (9.003%), showing a marked difference from the control, while the 80-ppm treatment generally resulted in a decline in the percentages of these compounds.

Interestingly, Geraniol exhibited a different response; its highest percentage was observed in the control group (14.666%), indicating a relative decrease in its synthesis under the influence of AuNP treatments. At a concentration of 60 ppm, the highest percentages of other phytochemicals were observed, specifically for Linalool (2.310%), cis-verbenol (1.919%), and Phytol (0.929%), exceeding the values found in all other treatments.

In summary, AuNPs functioned as effective biological elicitors, modulating the biosynthetic pathways of secondary metabolites in *Teucrium polium*. The results indicate that AuNPs can either enhance or suppress the synthesis of specific constituents depending on the compound type and the applied concentration. The 60-ppm concentration emerged as the optimal threshold for phytochemical enhancement, maximizing the yield of key bioactive compounds such as Citral E, Citral Z, geranyl acetate, phytol, linalool, and cis-verbenol. This peak suggests a saturation effect, where 60 ppm of AuNPs creates an ideal stimulatory environment that:

- Enhances the synthesis of secondary metabolites by activating defense-related biosynthetic pathways.

- Optimizes metabolic flux without inducing significant phytotoxicity.
- Avoids the inhibitory effects associated with nanoparticle aggregation, which was likely observed at concentrations exceeding 60 ppm.

While lower concentrations (<60 ppm) provided insufficient elicitation, higher concentrations (>60 ppm) appeared to inhibit yields, likely due to induced cellular stress. Therefore, 60 ppm represents the optimal balance where nanoparticle-plant interactions synergistically maximize phytochemical accumulation.

Table 3.
Impact of various synthesized AuNP concentrations on the percentage composition of *T. polium* plant essence constituents.

Compounds	Composition percentage at the different concentration (ppm)					
	0	**10**	**20**	**40**	**60**	**80**
Octan	1.60	1.31	13.61	0.39	-	21.03
1-Octen-3-ol	0.77	0.40	0.30	0.70	0.60	-
6-Methyl-5-hepten-2-one	1.04	0.64	0.95	1.00	0.82	1.04
Decane	1.15	-	4.60	0.65	0.60	7.44
2-Cyclohexen-1-one, 3-methyl	0.71	0.324	0.34	0.56	0.47	-
Linalool	0.78	0.524	0.44	0.53	0.93	-
Spiro[4.5]decan-7-one, 1,8-dimethyl-8,9-epoxy-4-isopropyl	0.60	0.50	0.20	-	-	-
Linalool formate	0.78	-	-	0.60	0.67	-
D(+)-10-Camphorsulfonyl chloride	0.40	-	-	0.60	0.48	-
Gerinic acid	-	-	1.00	3.13	-	-
Cis-Geranyl acetate	-	-	-	2.20	0.62	-
Caryophyllene	-	-	0.18	-	-	0.55
Cubebene	-	-	-	-	-	1.10

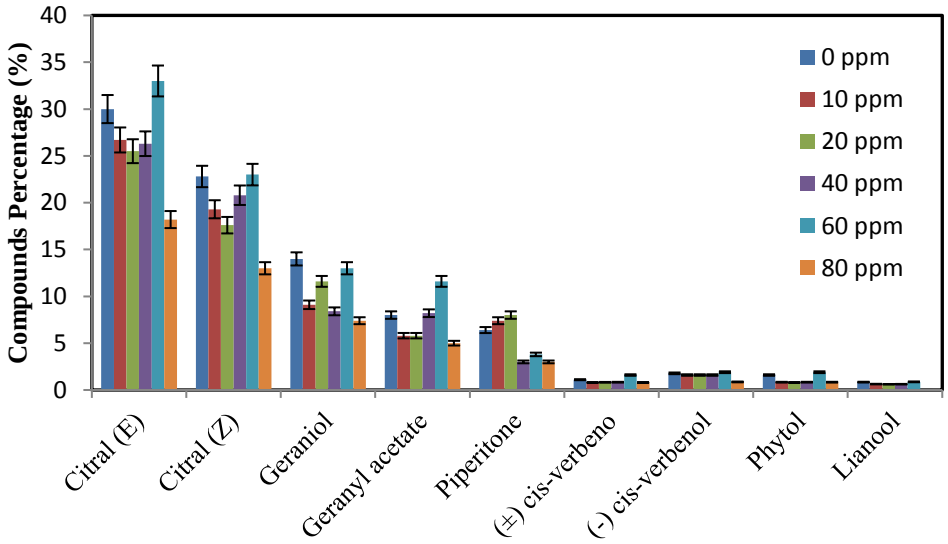

Figure 10. Distribution of chemical constituents in *T. polium* extract as influenced by different concentrations of synthesized AuNPs. *Data are presented as mean ± SD (n=3). Statistical significance was determined by one-way ANOVA ($p < 0.05$).

3.8. Antioxidant and reducing potential of *T. polium* extract across diverse AuNP treatments

The antioxidant capacity of *T. polium* plant extract under various AuNP treatments (0, 10, 20, 40, 60, and 80 ppm) was evaluated using the DPPH radical scavenging assay, with the resulting Half-Maximal Inhibitory Concentration (IC_{50}) values presented in Fig. 11. The IC_{50} values for the untreated extract (0 ppm) and the AuNP-treated samples were 11.81, 11.61, 10.48, 8.98, 9.94 and 12.67 μg/mL for the respective treatments. A notable reduction in IC_{50} values was observed in the 10, 20, 40, and 60 ppm groups compared to the control, indicating an enhancement in antioxidant properties. The highest antioxidant activity was recorded at 40 ppm, yielding the lowest IC_{50} value of 8.98 μg/mL. However, this trend reversed at 80 ppm, where the antioxidant activity significantly decreased. These results suggest that AuNPs exert a dose-dependent, bidirectional impact on the antioxidant potential of *T. polium*, where bioactivity is stimulated up to a specific concentration threshold before a subsequent decline occurs.

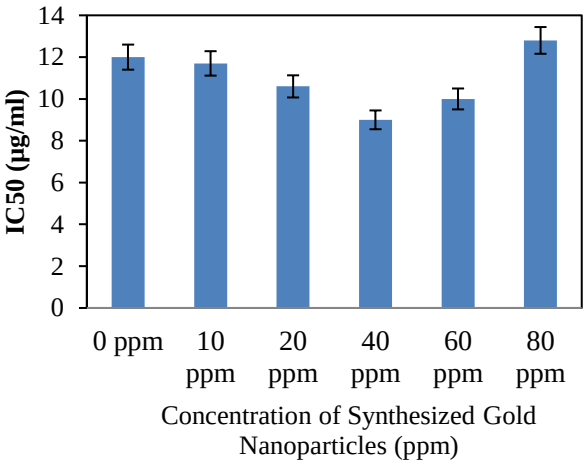

Figure 11. Evaluation of antioxidant capacity (IC50) for *T. polium* extract samples modified with different amounts of synthesized AuNPs. *Data are presented as mean ± SD (n=3). Statistical significance was determined by one-way ANOVA ($p < 0.05$).

To further validate these findings, the reducing power of the extract was assessed via the FRAP method (Fig. 12), using $FeSO_4 \cdot 7H_2O$ as the standard. Consistent with the DPPH results, the reducing power increased in the 10, 20, 40, and 60 ppm treatments relative to the untreated sample, peaking at 40 and 60 ppm with values of 16.71 and 16.85 mMFe2+/mg sample, respectively. The observed decrease in reducing power at 80 ppm further corroborates the bidirectional effect of AuNPs on the extract's antioxidant mechanisms.

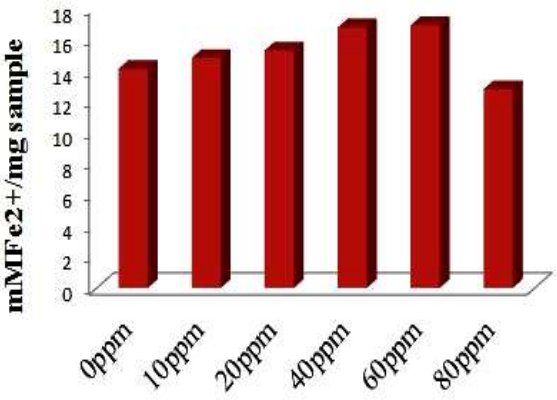

Figure 12. Effect of different synthesized AuNP concentrations on the reducing potential of *T. polium* extract samples.

Integrating these results with the GC-MS analysis, the 60-ppm concentration of AuNPs appears to represent the optimal threshold for enhancing the overall phytochemical profile of *T. polium*. While the maximum antioxidant activity IC_{50}) was observed at 40 ppm, the 60-ppm treatment maximized the yields of key bioactive compounds, including citral E, citral Z, geranyl acetate, phytol, linalool, and cis-verbenol. This suggests that at 60 ppm, AuNPs provide an optimal catalytic and stabilizing environment that maximizes extraction efficiency and the availability of these phytochemicals, potentially through enhanced interaction with plant cell membranes or modulation of biosynthetic pathways. The diminished yields and

bioactivity observed at concentrations exceeding 60 ppm (e.g., 80 ppm) may be attributed to nanoparticle aggregation or induced phytotoxicity, which could inhibit the stability of antioxidant compounds. Consequently, the 60-ppm concentration achieves the most favorable balance between phytochemical enrichment and biological efficacy, as evidenced by the near-maximum reducing power (16.85 mMFe2+/mg) and a competitive IC_{50} value (9.94 μg/mL).

3.9. Reproducibility of *T. polium* Extract-Mediated AuNPs Synthesis

To validate the reproducibility of the green synthesis method, three independent extractions and syntheses were performed using separate batches of *T. polium* plant material from distinct plants in Dashti County. Each batch was extracted independently, and the resulting extract was used for a separate synthesis to account for potential phytochemical variability. The synthesized nanoparticles exhibited consistent properties, as summarized in Table 4. The mean particle sizes (measured via TEM) ranged from 22.50 to 23.10 nm (overall mean: 22.83 ± 0.30 nm, CV=1.3%), with surface plasmon resonance (SPR) peaks at approximately 420 nm (UV-Vis) and spherical morphology (TEM). These results demonstrate the robustness and reproducibility of the synthesis method, making it suitable for scalable applications.

Table 4.
Reproducibility data for 3 independent syntheses

Batch	Mean Size (nm, TEM)	SD	SPR Peak (nm, UV-Vis)	morphology (TEM)
1	22.89	1.50	420	Spherical
2	23.10	1.80	418	Spherical
3	22.50	1.40	422	Spherical

4. Conclusions

Nanotechnology significantly influences plant physiology and the upregulation of secondary metabolites through the strategic application of nanomaterials. Such interventions allow for the precise modulation of growth-related genes and biosynthetic mechanisms.

In the present work, AuNPs were successfully synthesized via a sustainable green route employing *T. polium* extract as the reducing agent. The resulting nanoparticles exhibited a face-centered cubic (FCC) spherical morphology with a mean diameter of 22.89 nm, while their formation was further validated by a characteristic UV-Vis absorption maximum at 420 nm. This research assessed the antimicrobial potential of both *T. polium* extracts and their corresponding nanoparticles against a panel of fungal and bacterial strains. Furthermore, the impact of varying nanoparticle dosages (0–80 ppm) on phytochemical profiles was quantified via FRAP and DPPH assays. The analytical data yielded the following key observations:

- In terms of antimicrobial potency, the methanolic extract exhibited superior performance compared to the aqueous version, while AuNPs demonstrated the highest activity, particularly against *Aspergillus niger* and *Escherichia coli*.
- Phytochemical evaluations indicated that flavonoid concentrations and antioxidant capacities were enhanced by nanoparticle treatments up to 60 ppm, followed by a decline at 80 ppm. Notably, the maximum reducing power within the plant extract was achieved at a concentration of 40 ppm.
- Lower concentrations (<60 ppm) showed insufficient catalytic activation, while higher concentrations (>60 ppm) inhibited yields due to cellular stress.

- The findings demonstrate the efficacy of *Helpeh* ethanolic extract as an efficient reducing agent for AuNP fabrication, yielding nanoparticles with highly desirable dimensions.
- They also showed good antibacterial effects and can be considered as a suitable candidate for the development of antibacterial drugs for use in the food and pharmaceutical industries.
- Results demonstrated the robustness and reproducibility of the synthesis method, making it suitable for scalable applications.

  This study advances the current understanding of green nanotechnologies by demonstrating the efficacy of *T. polium* extracts in the synthesis of AuNPs. The resulting nanoparticles exhibit notable antibacterial activity, suggesting that this botanical-mediated method provides a viable, sustainable alternative for developing antimicrobial agents. Consequently, these findings open new avenues for the application of *T. polium*-derived AuNPs in the realms of nanomedicine and clinical antimicrobial research.

Abbreviation

OTC Over-The-Counter
DPPH 2,2-DiPhenyl-1-PicrylHydrazyl
ASA Ascorbic Acid
BHT Butylated Hydroxy Toluene
TPTZ 2,4,6-Tri(2-Pyridyl)-s-TriaZine
FCC Face-Centered Cubic
PDF Powder Diffraction File
ICDD International Center for Diffraction Data
GC-MS Gas Chromatography-Mass Spectrometry
IC50 Half-Maximal Inhibitory Concentration

Declarations of conflict of interest

The author declares that there is no conflict of interest.

CRediT authorship contribution statement

Ehsan Dahaz: Investigation.
Samer Asadi: Writing-review & editing, Writing-original, Conceptualization.
Somayeh Lashgari: Writing-review & editing.

Declaration of Competing Interest

The authors hereby certify that there are no financial conflicts of interest or personal affiliations that could be perceived as having influenced the findings or conclusions presented in this study.

Availability of data and materials

All data generated or analyzed in this study are included in this article.

References

[1] Panda, B., Rath, P.K., Mishra, B.P., et al. (2024). Novel Insights into the Antimicrobial Resistance and Strategies to Curb the Menace. J Pure Appl Microbiol, 18(1), 1-15. https://doi.org/10.22207/JPAM.18.1.42.

[2] Hayes, A., Zhang, L., Feil, E., Kasprzyk-Hordern, B., William, J.S., Gaze, H. (2025). Murray AK, Antimicrobial effects, and selection for AMR by non-antibiotic drugs in a wastewater bacterial community. Environment International, 199, 109490. https://doi.org/10.1016/j.envint.2025.109490.

[3] Zhang, X., Ding, W., Yang, J., Gao, L., Wang, Q., Wang, J., Luo, Y., Yuan, X., Sun, B., Yang, J., Zhou, Y., Sun, L. (2025). Mechanisms of outer membrane vesicles in bacterial drug resistance: Insights and implications. Biochimie, in press. https://doi.org/10.1016/j.biochi.2025.07.024.

[4] Abdullah, R., Younas, Q., Kaleem, A., Iqtedar, M., Aftab, M., & Saleem, F. (2024). Phytochemical and antimicrobial properties of different plants and *in silico* investigation of their bioactive compounds in wound healing and rheumatism. Saudi Journal of Biological Sciences, 31 (3), 103942. https://doi.org/10.1016/j.sjbs.2024.103942.

[5] Upadhyay, C., Vibha, Pathak, D., & Kulshreshtha, M. (2023). Preparation and evaluation of different herbal gels synthesized from Chinese medicinal plants as an antimicrobial agents. Pharmacological Research - Modern Chinese Medicine, 9, 100313. https://doi.org/10.1016/j.prmcm.2023.100313.

[6] Xia, M., Li, T., Ye, Y., Li, Y. (2025). Regrowth of AuNPsfacilitated utilizing small molecules ligand for high stability and performance. Chemical Engineering Journal, 508, 161086. https://doi.org/10.1016/j.cej.2025.161086.

[7] Salesa, B., Ferrús-Manzano, P., Tuñón-Molina, A., Cano-Vicent, A., Assis, M., Andrés, J., Serrano-Aroca, A. (2023). Study of biological properties of gold nanoparticles: Low toxicity, no proliferative activity, no ability to induce cell gene expression and no antiviral activity. Chemico-Biological Interactions, 382, 110646. https://doi.org/10.1016/j.cbi.2023.110646.

[8] Badoni, A., & Prakash, J. (2024). Noble metal nanoparticles and graphene oxide based hybrid nanostructures for antibacterial applications: Recent advances, synergistic antibacterial activities, and mechanistic approaches. Micro and Nano Engineering, 22, 100239. https://doi.org/10.1016/j.mne.2024.100239

[9] Hameed, S., Wang, Y., Zhao, L., Xie, L., Ying, Y. (2020). Shape-dependent significant physical mutilation and antibacterial mechanisms of AuNPsagainst foodborne bacterial pathogens (*Escherichia coli*, *Pseudomonas aeruginosa* and *Staphylococcus aureus*) at lower concentrations. Materials Science and Engineering: C, 108, 110338. https://doi.org/10.1016/j.msec.2019.110338.

[10] Gnanadesigan, M., Anand, M., Ravikumar, S., Maruthupandy, M., Vijayakumar, V., Selvam, S., Dhineshkumar, M., & Kumaraguru, A.K. (2011). Biosynthesis of silver nanoparticles by using mangrove plant extract and their potential mosquito larvicidal property. Asian Pacific Journal of Tropical Medicine, 4, 799-803. https://doi.org/10.1016/S1995-7645(11)60197-1.

[11] Sivakama, V.J., & Vaseeharan, B. (2012). Biosynthesis of silver nanoparticles by Cissus quadrangularis extracts. Materials Letters, 82, 171- 173. https://doi.org/10.1016/j.matlet.2012.05.040.

[12] Abdel-Aziz, M.S., Shaheen, M.S., El-Nekeety, A.A., Abdel-Wahhab, M.A. (2013). Antioxidant and antibacterial activity of silver nanoparticles biosynthesized using Chenopodium murale leaf extract. Journal of Saudi Chemical Society, 3, 1- 3. https://doi.org/10.1016/j.jscs.2013.09.011.

[13] Ávila-Avilés, R.D., Argueta-Figueroa, L., García-Contreras, R., & Vilchis-Nestor, A.R. (2024). Synthesis of biogenic silver and AuNPsfrom *Anemopsis californica* extract with antibacterial and cytotoxic activities. Materials Today Communications, 38, 108071. https://doi.org/10.1016/j.mtcomm.2024.108071.

[14] Dat, T.D., Cong, C.Q., Nhi, T.L.H., Khang, P.T., Nam, N.T.H., Tinh, N.T., Hue, D.T., & Hieu, N.H. (2023). Green synthesis of AuNPsusing *Andrographis paniculata* leave extract for lead ion detection, degradation of dyes, and bioactivities. Biochemical Engineering Journal, 200, 109103. https://doi.org/10.1016/j.bej.2023.109103.

[15] Bachman, S.P., Brown, M.J.M., Leão, T.C.C., Lughadha, E.N., Walker, B.E. (2024). Extinction risk predictions for the world's flowering plants to support their conservation, 566. https://nph.onlinelibrary.wiley.com/doi/full/10.1111/nph.19592.

[16] Nemati, S., et al. (2024). Effect of pH on the green synthesis of ZnO nanoparticles using Sorghum bicolor seed extract and their application in photocatalytic dye degradation. Journal of Hazardous Materials Advances, 372, 136966. https://doi.org/10.1016/j.hazadv.2024.136966.

[17] Gupta, A., Pandey, S., Variya, B., Shah, S., & Yadav, J.S. (2019). Green Synthesis of AuNPsUsing Different Leaf Extracts of Ocimum gratissimum Linn for Anti-tubercular Activity. Current Nanomedicine, 9(2), 146-157. https://doi.org/10.2174/2468187308666180807125058.

[18] Murugesan, P., & Moses, J.A. (2025). Carbon dot-assisted synthesis of AuNPsfor the development of a detection platform for trichlorfon. Next Materials, 8, 100691. https://doi.org/10.1016/j.nxmate.2025.100691.

[19] El-Said, W.A., Akhdhar, A., Al-Bogami, A.S., & Saleh, T.S. (2025). Design and green synthesis of carbon Dots/AuNPsComposites and their applications for neurotransmitters sensing based on emission Spectroscopy. Spectrochimica Acta, Part A: Molecular and Biomolecular Spectroscopy (SAA), 327, 125402. https://doi.org/10.1016/j.saa.2024.125402.

[20] Hutchinson, N., Wu, Y., Wang, Y., Kanungo, M., DeBruine, A., Kroll, E., Gilmore, D., Eckrose, Z., Gaston, S., & Matel, P. (2022). Green Synthesis of AuNPsUsing Upland Cress and Their Biochemical Characterization and Assessment. Nanomaterials, 12, 28. https://doi.org/10.3390/nano12010028.

[21] Kawsar, M., Hossain, M.S., Bahadur, N.M., & Ahmed, S. (2024). Synthesis of nano-crystallite hydroxyapatites in different media and a comparative study for estimation of crystallite size using Scherrer method, Halder-Wagner method size-strain plot, and Williamson-Hall model. Heliyon, 10(3), e25347. https://doi: 10.1016/j.heliyon.2024.e25347.

[22] Mekala, R., Thanishma Banu, N., Mathammal, R. (2025). Green synthesis of AuNPsusing Morinda citrifolia leaf extract: Its characterization and biological activities. Next Research, 2(3), 100629. https://doi.org/10.1016/j.nexres.2025.100629.

[23] Rehman, N., Shukla, S., Pandey, A., Anjana Pandey, A. (2025). Electrochemical sensing of 3,3'-Dichlorobiphenyl using green-synthesized AuNPsand Polyvinylpyrrolidone composite. Results in Chemistry, 16, 102364. https://doi.org/10.1016/j.rechem.2025.102364.

[24] Momeni, M., Asadi, S., Shanbedi, M. (2021). Antimicrobial Effect of Silver Nanoparticles Synthesized with Bougainvillea Glabra Extract on *Staphylococcus Aureus* and *Escherichia Coli*. Iranian Journal of Chemistry and Chemical Engineering (IJCCE), 40(2),

395-405. https://doi.org/10.30492/IJCCE.2020.97592.3369.

[25] Susanna, D., Balakrishnan, R.M., & Ettiyappan, J.P. (2023). Ultrasonication-assisted green synthesis and characterization of AuNPsfrom Nothapodytes foetida: An assessment of their antioxidant, antibacterial, anticancer and wound healing potential. Journal of Drug Delivery Science and Technology, 87, 104740. https://doi.org/10.1016/j.jddst.2023.104740.

[26] Safari-Talab, A., Asadi, S., & Lashgari, S. (2024). From nature to nanoparticles: Synthesizing silver nanoparticles from Moortalkh plant leaves with potent antibacterial properties. Inorganic Chemistry Communications, 165, 112458. https://doi.org/10.1016/j.inoche.2024.112458.

[27] Franzolin, M.R., Courrol, D.D.S., Silva, F.R.O., & Courrol, L.C. (2022). Antimicrobial Activity of Silver and AuNPsPrepared by Photoreduction Process with Leaves and Fruit Extracts of *Plinia cauliflora* and *Punica granatum*. Molecules, 27(20), 6860. https://doi.org/10.3390/molecules27206860.